Supplementary information

High-speed Electrodeposition of Copper-Tin-Zinc Layer Stacks from Liquid Metal Salts for $Cu_2ZnSnSe_4$ Solar Cells

M. Steichen, J. C. Malaquias, M. Arasimowicz, R. Djemour, N. R. Brooks, L. V. Meervelt, J. Fransaer, K. Binnemans, and P. J. Dale

Synthesis and characterization of tin containing materials

Chemicals:

SnO 99.9 % was purchased from Alfa Aesar. 1-methoxy-2-(2-methoxyethoxy)ethane (diglyme) 99% was purchased from Sigma-Aldrich. Hydrogen bis(trifluoromethylsulfonyl)imide was purchased from Iolitec (Heilbronn, Germany) as an 80 wt% solution in water.

Instrumentation:

DSC traces were recorded under a helium atmosphere using a Mettler-Toledo DSC822e module with a heating/cooling rate of 10 °C min^{-1}. The IR spectra were recorded in attenuated total reflectance mode on a Bruker Vertex 70 FTIR spectrometer at a resolution of 4 cm^{-1}. The viscosity of the fluid was measured at 80 °C on a Brookfield cone plate viscometer (LVDV-II+ programmable viscometer) with a cone spindle CPE-40. The measurement was performed under a dry nitrogen atmosphere, with a circulated water bath to control the temperature.

Reactions:

$[Sn(H_2O)_3][Tf_2N]_2$

SnO (12.32 g, 91.42 mmol) was added to a 80 wt.% aqueous solution of $H[Tf_2N]$ (34.3 g, 121.90 mmol) in water (100 mL). The reaction solution was stirred for 18 h at 100 °C, after which the remaining solid was

filtered off. The filtrate was removed on the rotary evaporator and the product was dried on a vacuum line overnight giving an off-white solid with a yield of 94%. CHN analysis: Calc. for $C4H_6F_{12}S_4O_{11}N_2Sn$: C, 6.55; H, 0.83; N, 3.82. Found: C, 6.36; H, 0.77; N, 3.60. IR (ATR, ν /cm^{-1}): 3382 (br), 1161, 1342, 1319, 1195, 1116, 1030, 792, 770, 737, 632, 609, 588, 571, 508.

[Sn(diglyme)(EtOH)][Tf_2N]$_2$

$[Sn(H_2O)_3][Tf_2N]_2$ (2.10 g, 2.87 mmol) was added to 1-methoxy-2-(2-methoxyethoxy)ethane (diglyme) (0.385 g, 2.87 mmol) dissolved in ethanol (20 mL) and was stirred for 1 h at room temperature. Ethanol was removed on the rotary evaporator and the product was dried overnight on a Schlenk line, yielding a viscous, transparent, pale yellow liquid. The product became solid after several days on the Schlenk line. The compound is hygroscopic and analyzed as $[Sn(diglyme)(EtOH)][Tf_2N]_2 \cdot 4H_2O$ during the CHN experiment as air exposure is unavoidable. For electrodeposition experiments the dried compound was immediately placed into an argon filled glove box. Melting point (DSC) = 59 °C. CHN analysis: Calc. for $C_{12}H_{28}F_{12}N_2O_{16}S_4Sn$: C, 15.48; H, 3.03; N, 3.01. Found: C, 15.40; H, 3.37; N, 3.14. IR (ATR, ν /cm^{-1}): 3305(br), 2951, 1458, 1406, 1336, 1185, 1129, 1049, 942, 861, 852, 822, 792, 766, 741, 605, 569, 410, 409.

$$[Sn(H_2O)_3][Tf_2N]_2 + G2 + \textit{EtOH} \not\rightarrow [Sn(G2)(\textit{EtOH})][Tf_2N]_2 + 3\ H_2O \quad \text{(Equation 1)}$$

Good quality single crystals were obtained after slow crystallization at room temperature on the vacuum line over a period of several days. For structural analysis, a single crystal was mounted on a nylon loop mounted on a copper pin and placed in the cold stream of an Oxford Cryostream 700 at 100(2) K on an Agilent SuperNova diffractometer using Mo Kα radiation (λ = 0.71073 Å). The absorption corrections were applied using CrysAlisPro.[1] The structure was solved using direct methods and refined by the full-matrix

least-squares procedure in SHELXL.[2] For refinement and making pictures, the program OLEX2 was used.[3] The hydrogen atoms for carbon were placed in calculated positions and refined using a riding model. The hydrogen atom on the oxygen of ethanol was found in the difference map and refined without restraints. The following final crystal data were obtained: Crystal Data for $C_{12}H_{20}F_{12}N_2O_{12}S_4Sn$ (M =859.23 g/mol): triclinic, space group P-1 (no. 2), a = 9.1134(3) Å, b = 9.5041(4) Å, c = 18.0048(7) Å, α = 85.032(3)°, β = 80.364(3)°, γ = 67.851(4)°, V = 1423.55(10) Å^3, Z = 2, T = 100(2) K, μ(MoKα) = 1.326 mm^{-1}, D_{calc} = 2.005 g/cm^3, 11850 reflections measured (5.68° ≤ 2Θ ≤ 58.06°), 6476 unique (R_{int} = 0.0207, R_{sigma} = 0.0327) which were used in all calculations. The final R_1 was 0.0518 (>2σ(I)) and wR_2 was 0.1129 (all data). CCDC-1452178 contains the supplementary crystallographic data for this paper. The crystallographic asymmetric unit consists of one [Sn(diglyme)(EtOH)] cation, one Tf_2N anion on a general position and two half Tf_2N anions positioned over crystallographic inversion symmetry sites (Figure S1). Because the Tf_2N anion cannot possess inversion symmetry these two are disordered (Figure S2). Restraints were required to keep the bond lengths and angles and the thermal parameters in the two disorder components similar. The ethyl group of ethanol was found to be disordered and modeled over two positions with the major component refining to be 84.9(9)% of the total. Restraints were required to keep the bond lengths and angles and the thermal parameters in the two disorder components similar. The Sn–O distance to ethanol was shorter than those to the diglyme oxygen atoms (Table S1), whilst the angles show a distorted T-shaped geometry (Table S2). There is also three longer Sn···O interactions to oxygen atoms of Tf_2N anions (Table S3). The O–H group of the ethanol molecule forms two hydrogen bonds but to the oxygen atoms of different disordered Tf_2N groups. Other than the hydrogen-bond, packing interactions are dominated by van der Waals interactions (Figure S3).

Table S1. Bond distances in the Sn coordination sphere.

	Distance / Å
Sn1–O1	2.229(3)
Sn1–O5	2.431(4)
Sn1–O8	2.348(4)
Sn1–O11	2.416(4)

Table S2. Bond angles in the Sn coordination sphere.

	Angle / °
O1–Sn1–O5	80.87(13)
O1–Sn1–O8	78.45(13)
O1–Sn1–O11	78.98(13)
O8–Sn1–O5	68.83(14)
O8–Sn1–O11	68.68(14)
O11–Sn1–O5	135.69(15)

Table S3. Long Sn···O interactions in the Sn coordination sphere.

	Distance / Å
Sn1–O19	2.937(4)
Sn1–O22	2.690(4)
Sn1–O71^{i}	2.992(9)

Symmetry code: (i) 1-*x*,1-*y*,-*z*

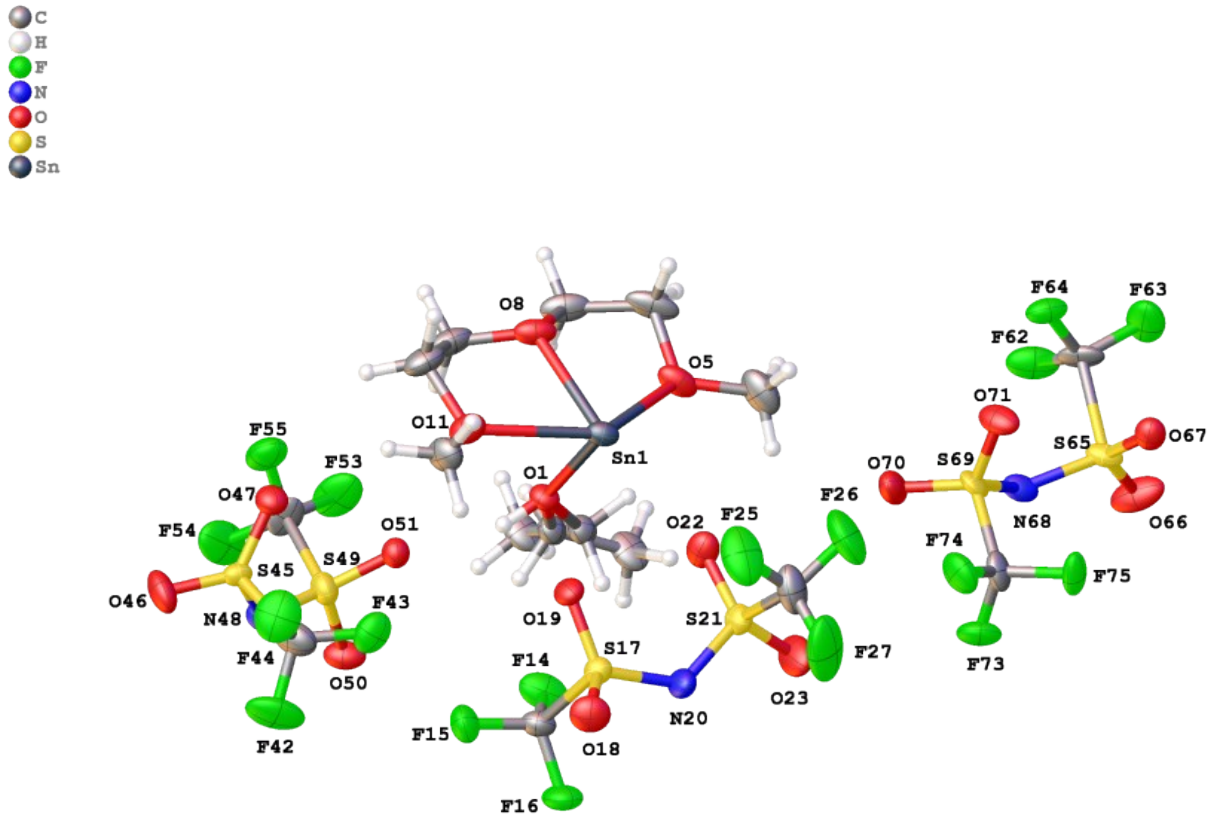

Figure S1. View of the crystal structure of [Sn(diglyme)(EtOH)][Tf_2N]$_2$ showing the disorder of the EtOH molecule and the three independent Tf_2N anions, two of which are half occupied because they occupy inversion symmetry sites in the structure (those numbered C41–F55 and C61–F75). Displacement ellipsoids are shown at the 50% probability level.

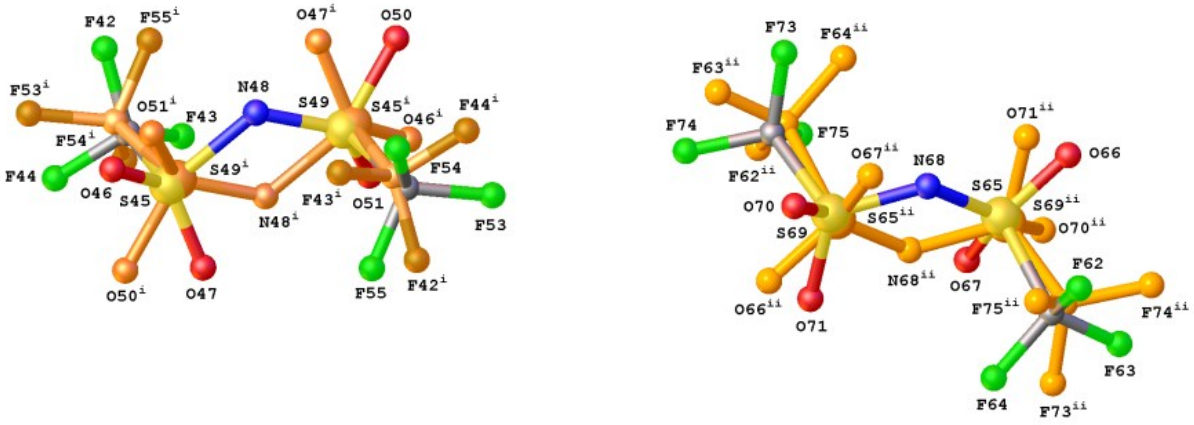

Figure S2. View of the crystal structure of [Sn(diglyme)(EtOH)][Tf_2N]$_2$ showing the two disordered Tf_2N anions which occupy inversion symmetry sites in the structure. Displacement ellipsoids are shown at the 50% probability level. Symmetry codes: (i) 1-*x*,2-*y*,1-*z*; (ii) 1-*x*,-*y*,-*z*.

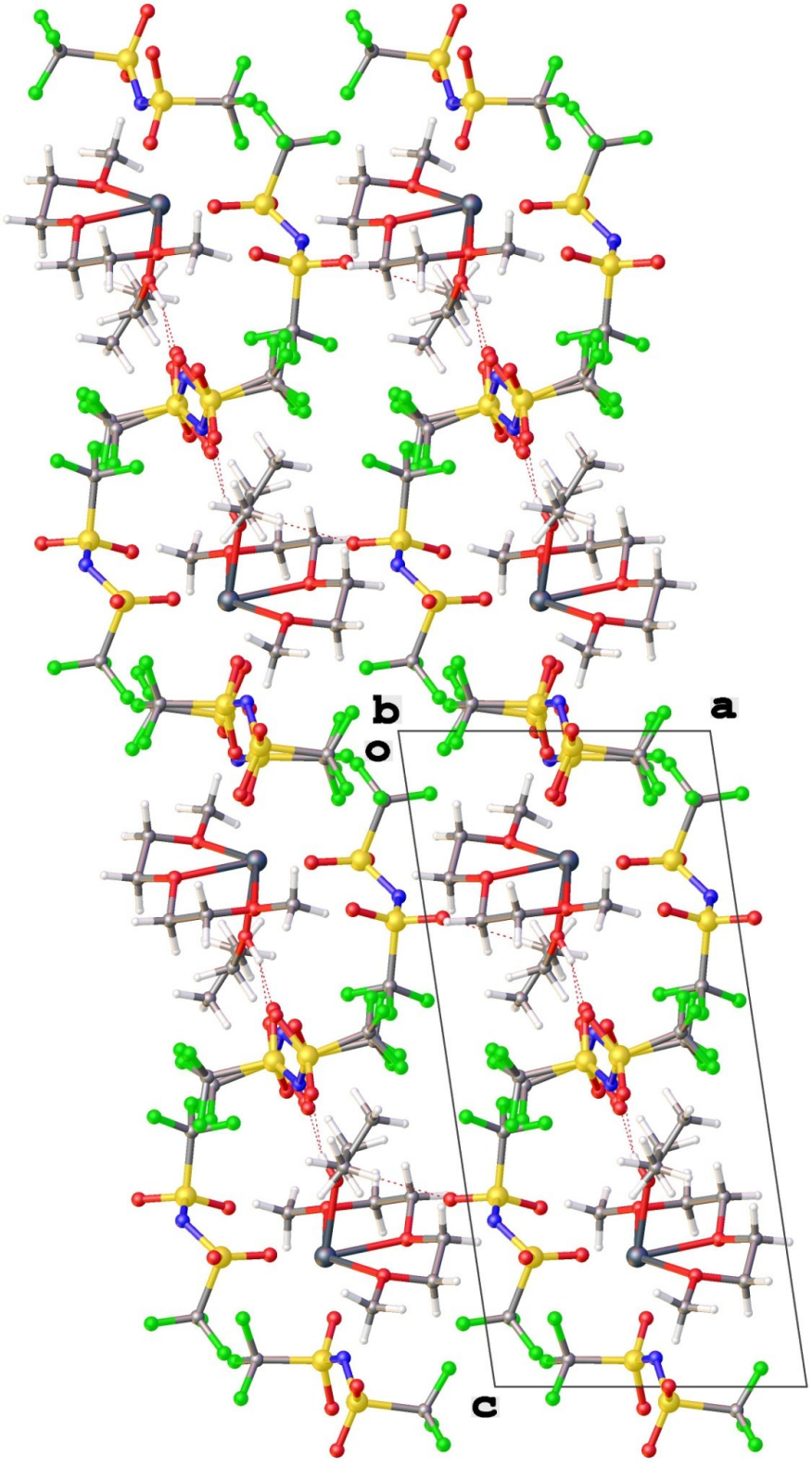

Figure S3. View of the packing in the crystal structure of [Sn(diglyme)(EtOH)][Tf_2N]$_2$.

$Cu_2ZnSnSe_4$ formation

Chemicals

$[Cu(MeCN)_4][Tf_2N]$ (MeCN = acetonitrile), $[Sn(G2)(EtOH)][Tf_2N]_2$ (G2 = 1-methoxy-2-(2-methoxyethoxy)ethane or diglyme; EtOH = ethanol), $[Zn(EtIm)_6][Tf_2N]_2$ (EtIm = 1-ethylimidazole) were all synthesized in our laboratory. Mo coated glass was prepared in house, and tin selenide and selenium power were obtained from Alfa Aesar (both 99.999%).

Characterization

Scanning electron microscopy (SEM) was performed on an Hitachi SU-70, equipped with an Oxford Instruments INCA X-MAX analyzer for Energy Dispersive X-ray Spectroscopy (EDX).

Grazing incidence X-ray diffraction patterns for the metallic precursor and absorber were measured using a Bruker D8 Discovery diffractometer. The Cu Kα radiation (λ = 1.5418 Å) was used. The reference diffraction patterns used are from the 2013 ICDD database.

Raman spectroscopy was measured in a custom made setup, using an argon ion laser 457.9 nm line.

Electrodeposition of Cu/Sn/Zn precursor layers

Electrochemical experiments were performed in a nitrogen-filled glove box with oxygen and water levels below 1 ppm. The working electrode consisted of a molybdenum layer sputtered on soda lime glass (Mo-SLG) with a geometrical surface area of 2 x 2 cm^2. The temperature-controlled (90 °C) cell was connected to an Ecochemie Autolab PGSTAT302N potentiostat, equipped with GPES software for cyclic voltammetry and galvanostatic electrodeposition experiments. The galvanostatic deposition of the Cu, Sn and Zn layers were performed at a cathodic current j = - 200 $mA.cm^{-2}$. High purity, large area copper, tin and zinc metal wires (diameter = 3 mm) served as counter and reference electrodes (pseudo-reference) in their corresponding liquid metal salts. Uniform primary current density distribution over the working electrode

surface was achieved by channeling the current density lines in the deposition cell setup. Prior to use, the Mo-SLG substrates were etched in an aqueous 30 % ammonia solution for 5 min, ultrasonically cleaned in water and ethanol and dried under a nitrogen flow. The working electrodes were washed with ethanol and dried under nitrogen to avoid any cross-contamination of the individual liquid metal salts. After electrodeposition the Mo/Cu/Sn/Zn metal stacks were stored under vacuum before further processing.

The SEM images of the top surface of the deposits are shown in Figure S4 below. The copper layer is smooth and compact with grain sizes of approximately 200 nm. The Sn on Cu layer is less compact than the Cu with grain sizes of around 1 micron. The Zn does not form a continuous layer on the surface, rather only scattered grains of several microns in size.

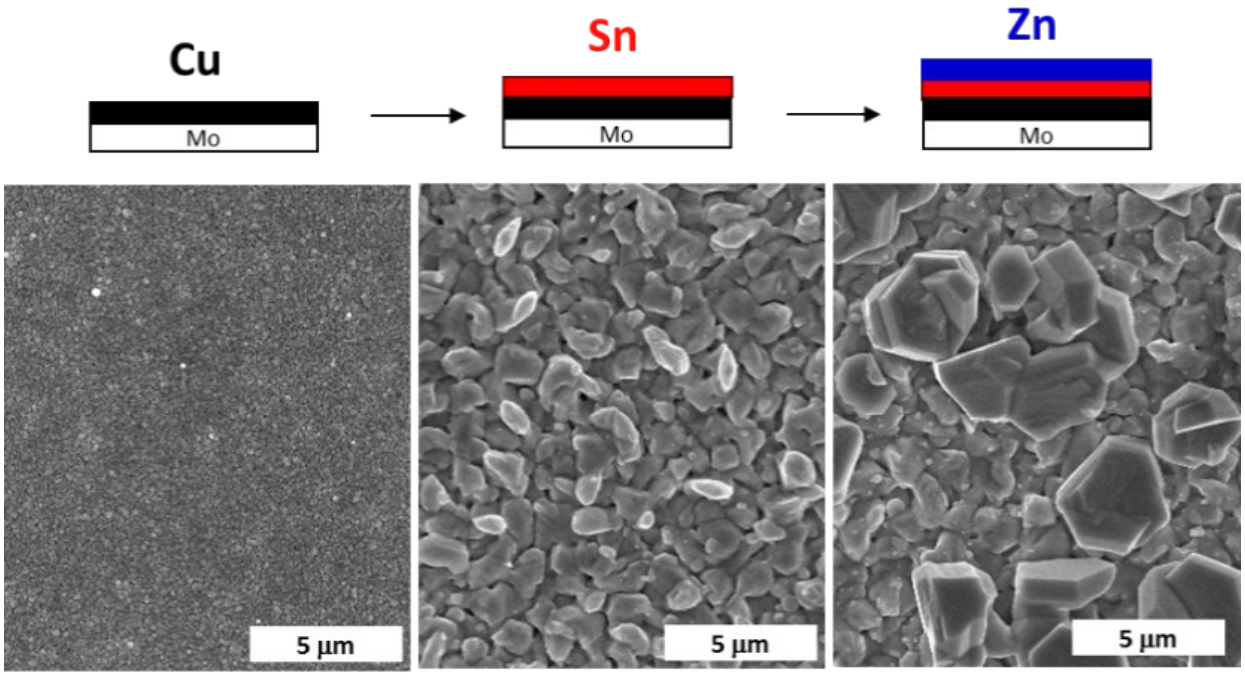

Figure S4. SEM top down images of Cu (left), Sn on Cu (middle), and Zn on Sn on Cu layers (right) electrodeposited from the liquid metal salts. All layers were deposited galvanostatically with a deposition current of -200 mA cm^{-2} at 90°C.

XRD of as deposited metallic precursor

The X-ray diffraction pattern of the as-deposited Cu/Sn/Zn metallic precursor is shown in Figure S5. All peaks can be assigned to the substrate Mo, Cu, Sn, Zn, and Cu_6Sn_5. This suggests little to no alloying between Cu and Zn during the deposition, presumably due to the very short deposition times.

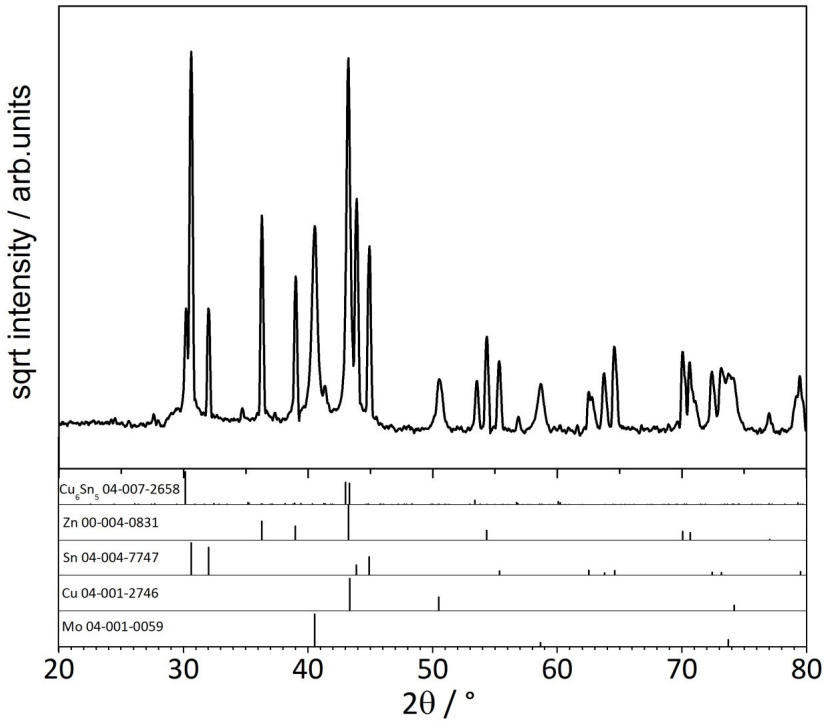

Figure S5. X-ray diffractogram of the as-deposited Cu/Sn/Zn stack on Mo. Below the diffractogram are JCPDS reference files for the observed phases.

Characterization of the absorber by x-ray diffraction

Figure S6 shows the GIXRD from the absorber layer adjacent to the best working device along with reference patterns for all the expected secondary phases. All major and minor peaks of kesterite are present in the diffractogram. The presence of Cu_2SnSe_3 cannot completely be ruled out by GIXRD alone since it shares several peak positions with kesterite. However, given the zinc-rich nature of the absorber layer and the absence of the Cu_2SnSe_3 peaks in the Raman spectrum, its presence is extremely unlikely. Additionally the presence of ZnSe, Cu_2Se and SnSe are also ruled out. Note that Raman spectroscopy can be more sensitive than XRD at detecting small quantities of ZnSe.

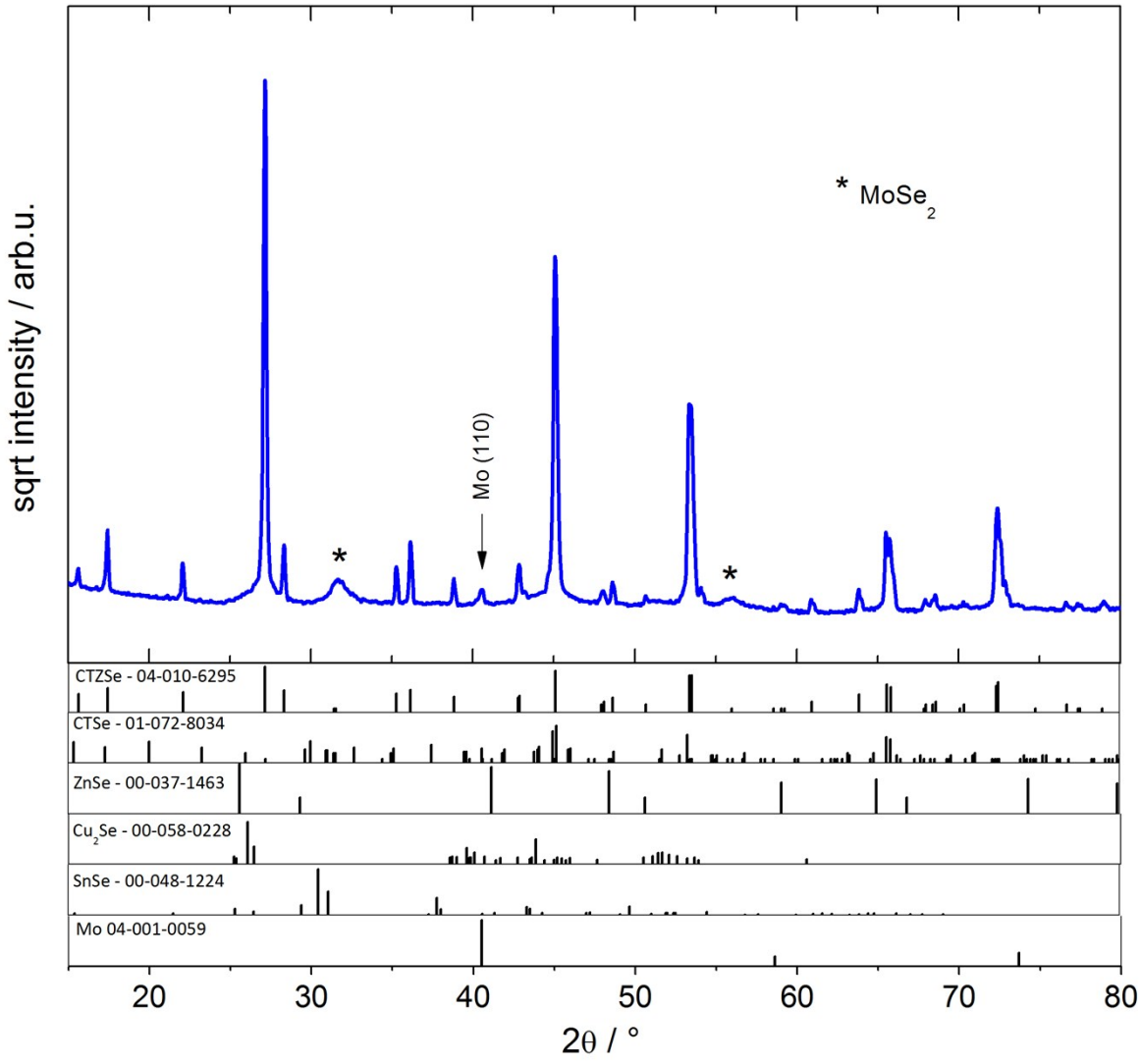

Figure S6. Grazing incidence X-ray diffractogram (GIXRD) of a kesterite absorber layer synthesized from liquid metal salt electrodeposited precursor annealed in the rapid annealing furnace. The diffractogram is

compared reference ICDD powder diffraction files of kesterite, the most likely secondary phases and the molybdenum, the substrate.

$Cu_2ZnSnSe_4$ semiconductor absorber preparation

Prior to selenization, the electrodeposited Cu/Sn/Zn metal precursors were pre-annealed during 30 min in a rapid thermal processing oven Annealsys AS-One 100 at 350 °C, under a nitrogen atmosphere. Further experiments showed that one minute is sufficient for this alloying treatment. Selenization of the alloyed precursor was carried out in the same rapid thermal annealing oven in the presence of Se and SnSe, during four minutes at 550 °C and under a H_2/N_2 10%/90% atmosphere.

Characterization of the absorber by SEM and energy dispersive x-ray spectroscopy (EDX)

A representative image of the surface of the absorber layer adjacent to where the best device was fabricated is given in Figure S7.

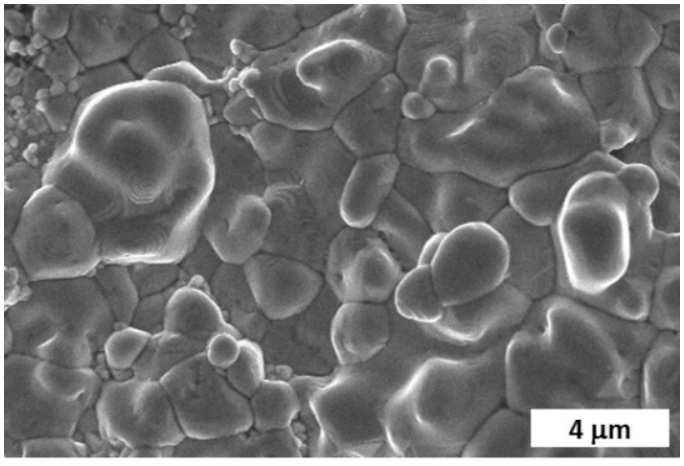

Figure S7. SEM top down image of an annealed kesterite layer. The large grains are kesterite, whilst the small grains in the top left of the image are most likely ZnSe [4].

The absorber layer adjacent to the best work device was analyzed by EDX over a 400 x 400 µm area using an accelerating voltage of 20 kV. The degree of uncertainty for the atomic percentage is estimated to be ± 1 % absolute.

Cu (at%)	Zn (at%)	Sn (at%)	Se (at%)	Cu/(Zn+Sn)	Zn/Sn	Se/(Cu+Zn+Sn)
23.8	15.0	12.1	49.1	0.88 ± 0.10	1.24 ± 0.13	0.96 ± 0.11

Characterization of the absorber by secondary ion mass spectrometry (SIMS)

Secondary ion mass spectrometry (SIMS) measurements were performed using a CAMECA SCUltra instrument. The in-depth composition profiles were obtained by bombarding the layers with $^{133}Cs^{+}$ ions, with 4.5 kV acceleration. To minimize matrix effects, copper, zinc, tin, molybdenum and oxygen were measured as metal cesium ion clusters, respectively.

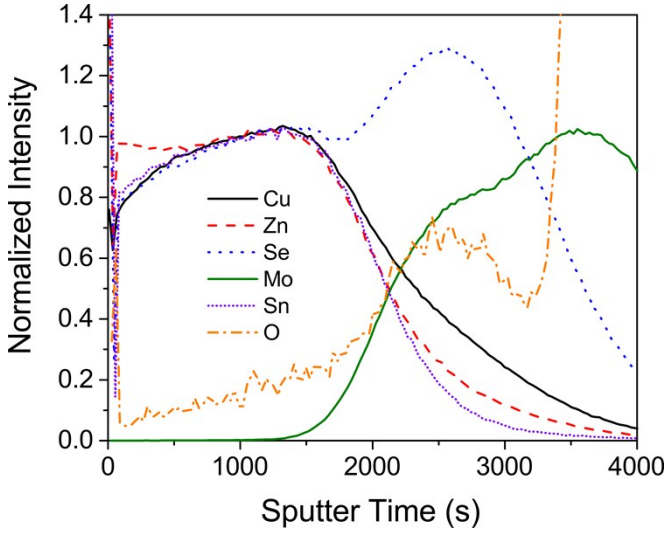

Figure S8. Secondary ion mass spectrometry Cu, Zn, Se, Mo, Sn and O profiles of the CZTSe absorber layer which delivered the most efficient device. Cu, Sn, Zn, and Se intensities were normalized to one at approximately the onset of the Mo substrate signal.

Solar Cell preparation

Characterization

All current-voltage (*j-V*) measurements were performed in a custom made setup, where a halogen lamp of intensity 1000 $W.m^{-2}$ was used to simulate the AM1.5 spectrum. Prior to measuring the *j-V* curve, the system was calibrated using a monocrystalline silicon solar cell with known and well-defined short circuit current.

External quantum efficiency measurements (EQE) were performed in a custom-made setup, using a halogen and a xenon lamp as light sources. The spectral response was calibrated using a Si and an InGaAs photodiodes.

Fabrication

Solar cells were fabricated from the absorber layers according to the following procedure: a 50 nm CdS layer was deposited by chemical bath deposition on top of the absorber, followed by the deposition of an 80 nm intrinsic ZnO layer and of a 380 nm Al-doped ZnO layer by sputtering. Ni-Al electric contacts with a thickness of 2 µm were deposited by electron beam evaporation. A cross sectional SEM and an explanatory schematic of the final device is show in Figure S9. The absorber layer is approximately 2 µm thick.

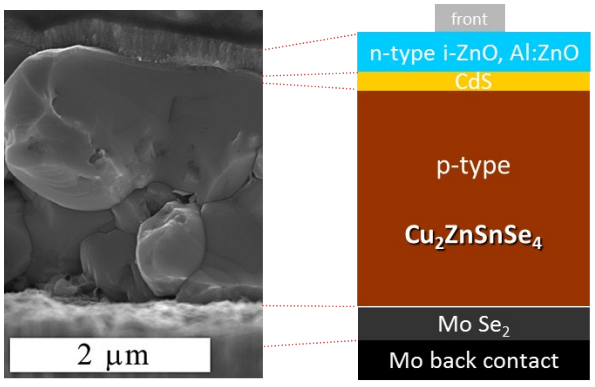

Figure S9: SEM cross section (left) and cartoon of the full device structure (right).

References

1 CrysAlisPro, Agilent Technologies, Yarnton, UK, 2015.
2 G. M. Sheldrick, *Acta Crystallogr., Sect. C: Struct. Chem.*, 2015, 71, 3 – 8.
3 A. V. Dolomanov, L. J. Bourhis, R. J. Gildea, J. A. K. Howard and H. Puschmann, *J. Appl. Crystallogr.*, 2009, 42, 339.
4 D. Colombara, E. V. Robert, A. Crossay, A. Taylor, M. Guennou, M. Arasimowicz, J. Malaquias, R. Djemour, P. J. Dale, *Sol. Energ. Mat. Sol. Cells* 2014, 123, 220–227